

Ferroelectric stripe domains in PbTiO₃ thin films: Depolarization field and domain randomness

R. Takahashi,^{a)} Ø. Dahl, E. Eberg, J. K. Grepstad, and T. Tybell^{b)}

Department of Electronics and Telecommunications, Norwegian University of Science and Technology, O. S. Bragstads plass 2a, 7491 Trondheim, Norway

(Received 14 March 2008; accepted 17 July 2008; published online 22 September 2008)

Observation of stripe domains in PbTiO₃ thin films using standard x-ray diffraction analysis at room temperature is discussed. High-quality *c*-axis oriented thin films of varying thickness, from 6 to 210 unit cells, were grown on buffered NH₄-HF etched SrTiO₃(001) and Nb:SrTiO₃(001) substrates using off-axis radio frequency magnetron sputtering. High-resolution linear Q_x scans reveal a superstructure around the specular Bragg peaks, consistent with the presence of ferroelectric stripe domains. For thin samples, the stripe width is found to be proportional to the square root of the film thickness, with random in-plane orientation of domains. For films with a thickness of more than ~ 100 unit cells, both monodomain samples and stripe domains were observed. We present evidence for the presence of a threshold depolarization field, above which there is a monotonically decreasing relationship between the domain width and the depolarization field. Furthermore, simulations show that random variations in size of the domains affect the separation of the diffuse scattering peaks from that of the specular reflection. © 2008 American Institute of Physics.

[DOI: [10.1063/1.2978225](https://doi.org/10.1063/1.2978225)]

I. INTRODUCTION

The ferroelectric domain structure of perovskite epitaxial films has attracted extensive scientific interest in recent years,^{1–4} specifically the 180° stripe domains of alternate “up” and “down” polarizations arranged in an “in-plane superlattice” fashion.^{5–15} These stripe domains serve to minimize the total free energy, including contributions from depolarization field and domain walls.^{5,6} In ultrathin films, the depolarization field is strongly enhanced, which causes a breakdown of the ferroelectric state below some critical film thickness.^{16,17} Studies of the intrinsic domain structure in such films may thus help to elucidate the possibility of nanoscale ferroelectricity.^{1–4} For example, Fong and co-workers^{7,8} showed that a 3 unit cell thick film of PbTiO₃ can be ferroelectric, based on stripe domain observations in such films using synchrotron x-ray diffraction (XRD) techniques. The debate on stripe domains in ferroelectric thin films has been focused on the interplay between crystal symmetry and stripes,⁹ how the film thickness affects the domain state,^{10,11} photochemically induced stripe to monodomain transition coupled with a change in crystal symmetry,¹² and how electrostatic boundary conditions can be used to tailor the domain ground state.^{13–15} In all of these studies, it is evident that the depolarization field plays a crucial role in the formation of ferroelectric domains.

In this paper, we focus on the observation of stripe domains in PbTiO₃ thin films deposited on substrates of SrTiO₃ and Nb-doped SrTiO₃, using a standard XRD instrument. In

particular, we discuss the relationship between depolarization field and the average stripe width. We show that randomness in the domain periodicity affects the stripe width estimates, and that samples with a large preferential polarization, up to at least 90%, can give rise to the Bragg peak superstructure characteristic of the ferroelectric stripe domain ground state.

II. EXPERIMENT

The PbTiO₃ samples were grown by off-axis magnetron sputtering on (001)-oriented SrTiO₃. Both insulating substrates pretreated with buffered NH₄HF for a well-defined surface termination¹⁸ and annealed conducting substrates doped with 0.5 wt % Nb were used. A composite PbTiO₃ sputter target with 10 % excess lead was used. The samples were deposited in a 165 mTorr O₂:Ar (4:10) ambient. The growth temperature was 510–530 °C, as measured with an optical pyrometer with the emissivity set at 0.7. The film thickness was varied between 2.4 and 94.2 nm, as determined from low-angle reflectometry measurements and the thickness fringes observed around the (001), (002) reflections in the θ - 2θ x-ray diffractograms [see Figs. 1(a)–1(c)], as measured with a Bruker D8 Discover diffractometer. Rocking curve measurements on the (001) reflection typically displayed a full width at half maximum (FWHM) of less than 0.03° throughout this study. The measured (001) lattice parameter varied as a function of film thickness, from 4.16 Å for thick samples down to 4.00 Å for the thinnest samples, in accordance with previously reported values.^{17,19} In-plane epitaxy is inferred from phi scans recorded for the (101) reflections of the PbTiO₃ film and the SrTiO₃ substrate, displayed in Figs. 1(d) and 1(e). Figure 2 shows a reciprocal space map for the (103) PbTiO₃ and Nb:SrTiO₃ reflections. The in-plane lattice constant of PbTiO₃ corre-

^{a)}Present address: Department of Materials Science and Engineering, University of Maryland, College Park, MD 20742, USA. Electronic mail: ryota@umd.edu.

^{b)}Author to whom correspondence should be addressed. Electronic mail: thomas.tybell@iet.ntnu.no.

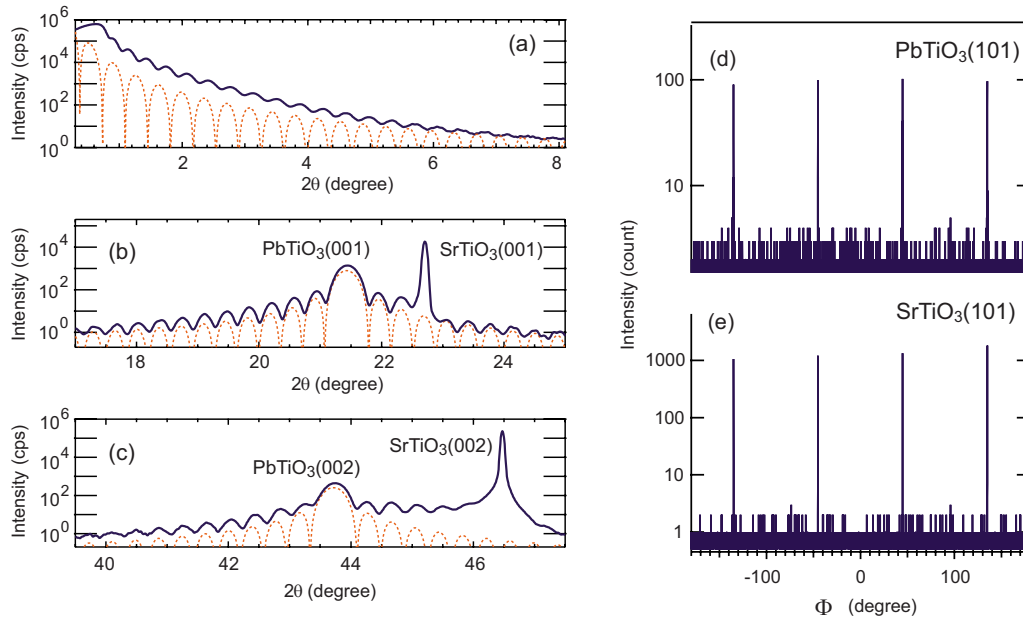


FIG. 1. (Color online) θ - 2θ XRD diffractograms of a 60 unit cell thick film of $\text{PbTiO}_3/\text{SrTiO}_3$ at low-angle (a), and around the (001) (b) and (002) (c) Bragg reflections, respectively. (d) and (e) show phi scans of the (101) reflections for PbTiO_3 and SrTiO_3 , respectively.

sponds to that of the $\text{Nb}:\text{SrTiO}_3$ substrate. Thus coherent growth of PbTiO_3 on $\text{Nb}:\text{SrTiO}_3$ was verified for samples up to 94.2 nm in thickness.

Figures 3(a) and 3(b) show typical atomic force microscopy (AFM) images of the PbTiO_3 films with atomically smooth surfaces in a step-and-terrace structure, the steps corresponding to 1 unit cell of PbTiO_3 . The high-resolution AFM micrograph inserted in Fig. 3(a) reveals a repetitive structure of islands superimposed on the terraces. This high quality film surface morphology was confirmed by plane-view high-resolution transmission electron microscopy (HRTEM), as shown in Fig. 3(c).

Electrical characterization measurements were performed on 100 nm thick films using a commercial ferroelectric tester (aixACCT TF analyzer 2000). Figures 4(a) and

4(b) show typical polarization versus electric field hysteresis loops and displacement current versus electric field results. To this end, a 200 nm Au/50 nm Pt top electrode was deposited and defined using a stencil mask with typically 100 μm diameter. The conducting $\text{Nb}:\text{SrTiO}_3$ substrate served as bottom electrode, contacted with a Ti/Au layer. The samples examined in this study typically displayed a built-in bias of 200 kV/cm, as seen in Fig. 4. The switchable polarization at zero bias was measured at 25.3 $\mu\text{C}/\text{cm}^2$.

III. RESULTS AND DISCUSSION

High-resolution linear Q_x scans around the (001) reflection reveal two satellite peaks, separated by the same ΔQ_x on either side of the specular reflection and with approximately two orders of magnitude reduced intensity. Figure 5 displays the in-plane x-ray scattering profiles recorded for the PbTiO_3 Bragg peaks with Miller indices (001), (003), (103), and (303), for a 58 unit cell thick film grown on SrTiO_3 . The satellite peaks are clearly visible for all reflections examined. Moreover, the measured values of ΔQ_x are the same for every investigated (hkl) reflection in reciprocal space.

It is known that both a -axis oriented inclusions and misfit dislocations at the interface between film and substrate

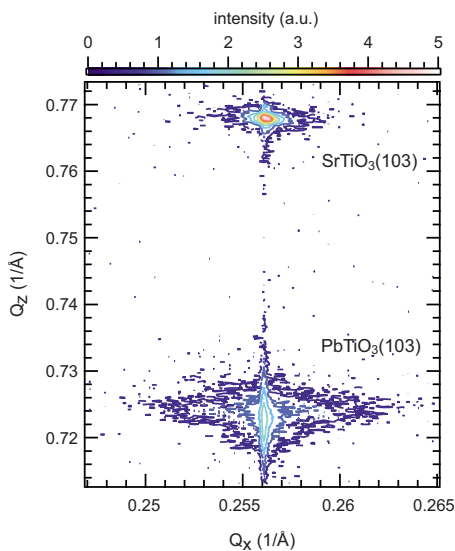


FIG. 2. (Color online) Reciprocal space map of the (103) Bragg reflection for a 80 nm thick film of $\text{PbTiO}_3/\text{Nb}:\text{SrTiO}_3$.

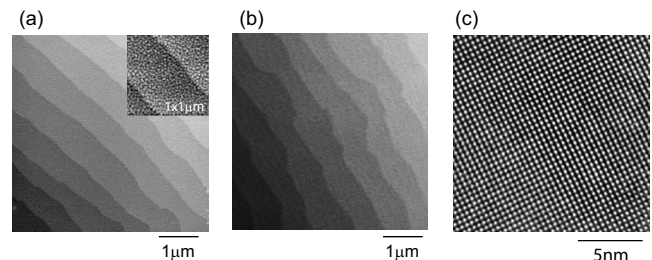


FIG. 3. AFM images of a 14 unit cell (a) and a 105 unit cell (b) thick film of $\text{PbTiO}_3/\text{Nb}:\text{SrTiO}_3$. (c) shows a plane-view TEM image of a 27 unit cell thick film of $\text{PbTiO}_3/\text{SrTiO}_3$.

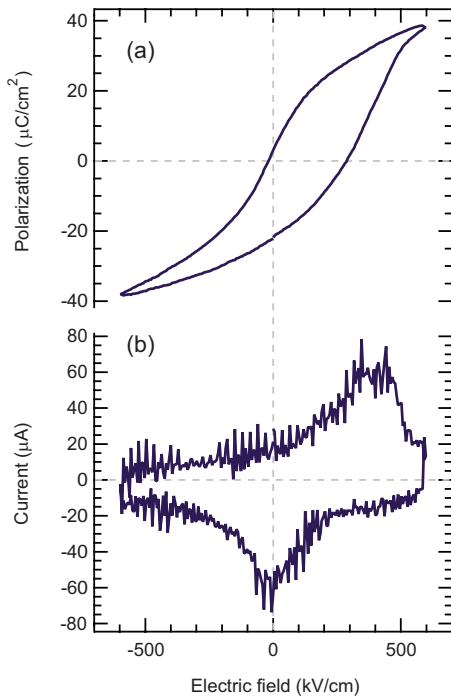


FIG. 4. (Color online) A typical ferroelectric hysteresis loop (a) and displacement current vs electric field (b) for a 100 nm thick film of $\text{PbTiO}_3/\text{Nb}:\text{SrTiO}_3$.

may give rise to satellite peaks in linear Q_x scans.^{20,21} Cross-section HRTEM and scanning TEM studies on similar samples²² did not reveal the presence of any such defects, ruling out formation of a -axis oriented domains as the origin of the satellite peaks in the recorded XRD data.^{20,21} Kaganer *et al.*²³ stated the following two criteria that must be fulfilled in order for the observed satellite peaks to be explained by misfit dislocations: (1) the Burgers vector should not be confined to the interface plane, and (2) the product of misfit dislocation density (ρ) with film thickness (d) should be small, i.e., less than 0.5 for 60° dislocations. With a tensile lattice mismatch of 0.15% for PbTiO_3 on SrTiO_3 at room temperature,^{24,25} the ρd product will be less than 0.5 for all film thicknesses investigated in this study. However, we note that PbTiO_3 on SrTiO_3 is reported to have edge dislocations with Burgers vectors of type $\langle 100 \rangle$,²⁶ excluding misfit dislocations as the origin of the observed satellite peaks.

In order to rule out those superimposed islands on the step-and-terrace film surface as the origin of the satellite peaks in the linear Q_x scans,^{27,28} high-resolution AFM data, cf. the inset in Fig. 3(a), was subjected to a two-dimensional (2D) fast Fourier transform (FFT) analysis, as displayed in Fig. 6(a). The corresponding linescan in Fig. 6(b), with the fitted Voigt functions, serves to expose the in-plane modulation of the AFM image. The 2D FFT data unveil a surface modulation period of 50 nm, in addition to the peaks from the step-and-terrace structure. The characteristic length scale of this surface modulation is independent of the film thickness, cf. Fig. 6(c), possibly increasing for samples thicker than 100 unit cells. Figure 6(c) also displays the modulation derived from the linear Q_x scans of the same samples. These data uncover a striking difference in the film thickness dependence for the two characterization techniques; the modu-

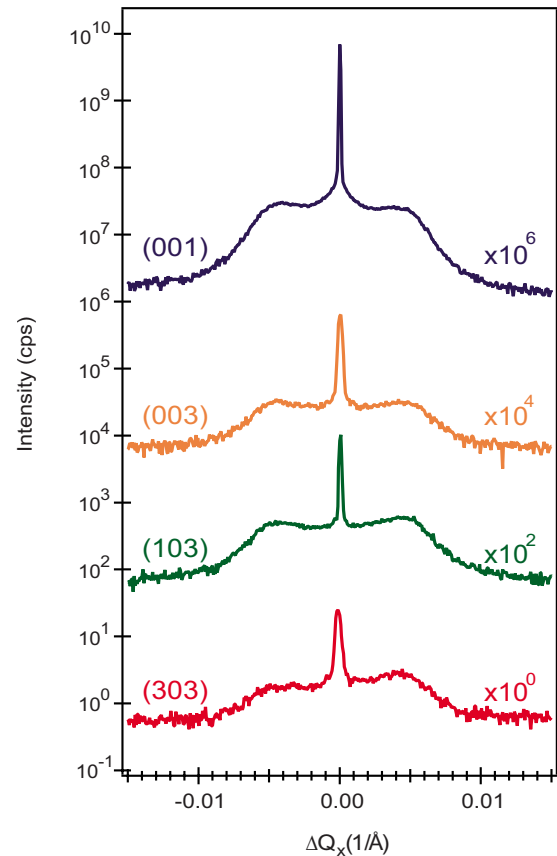


FIG. 5. (Color online) High-resolution linear Q_x profiles recorded for the (001), (003), (103), and (303) reflections of a 58 unit cell thick film of $\text{PbTiO}_3/\text{SrTiO}_3$.

lation period increasing monotonically when probed with XRD, while remaining virtually unaffected by the film thickness when determined from AFM. This finding suggests that the topographic modulation of the film surface is not the origin of the observed satellite peaks in XRD.

Figure 6(d) depicts the XRD satellite and specular peak intensities normalized to the respective substrate peaks for films deposited on SrTiO_3 and $\text{Nb}:\text{SrTiO}_3$, as a function of film thickness. The increasing intensity of the specular peak is proportional to the film thickness squared, for samples grown on both substrates. A similar trend is found for the diffuse satellite peak intensities in films grown on conductive $\text{Nb}:\text{SrTiO}_3$. For samples grown on SrTiO_3 substrates, we note a possible deviation for film thicknesses in excess of ~ 60 unit cells. However, the closely corresponding thickness dependence of the specular and diffuse reflections suggests that the diffuse peaks derive from a bulk effect, consistent with the preceding discussion of the AFM data.

A possible bulk scenario is the presence of 180° ferroelectric stripe domains. In this scenario, the separation in reciprocal space between the diffuse satellite peaks and the corresponding specular reflection, ΔQ_x , is inversely proportional to the in-plane modulation of the XRD structure factor, which in turn depends on the polarization state with P_{up} different from P_{down} .²⁹ We note that the measured ΔQ_x remains fixed independent of the selected Bragg reflection for the Q_x -scans in Fig. 5, strongly suggesting a modulation of the structure factor. Hence, we attribute the recorded satellite

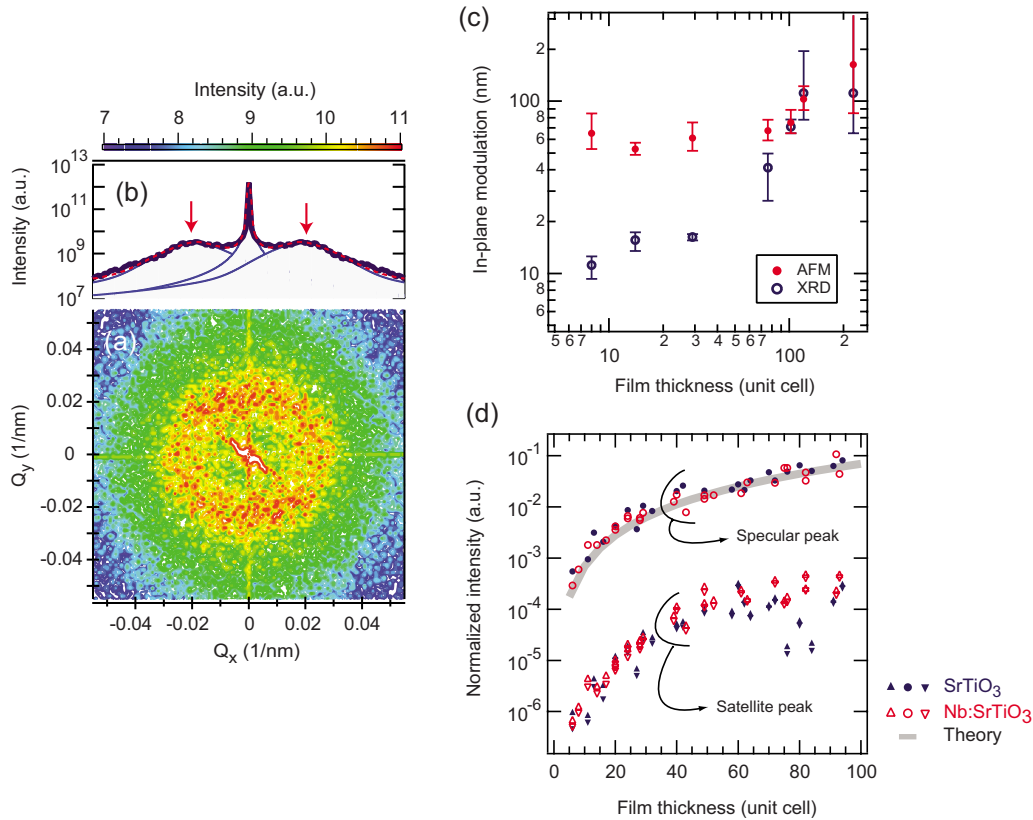


FIG. 6. (Color online) (a) 2D FFT of an AFM image equivalent to that displayed in the inset of Fig. 3(a). (b) Q_x profile of this 2D FFT, fitted by Voigt functions. (c) Film thickness dependence of the in-plane surface modulation. (d) Film thickness dependence of the XRD intensities of corresponding Bragg and satellite peaks.

peaks of the in-plane scattering profiles to ferroelectric stripe domains with a well-defined period, reflecting the modulation of the XRD structure factor with domain polarity, as illustrated in Fig. 7(a). From the peak intensity profiles in Fig. 5, the characteristic stripe width for this 58 unit cell thick film is estimated at 24.6 nm by fitting of Voigt functions to the recorded Q_x -scans.

The structure factor difference between up and down domains can have various manifestations, such as anomalous dispersion effects, where the absorption of the noncentrosymmetric unit cell of ferroelectric materials is different for up and down domains,^{30,31} or interference effects with the substrate.²⁹ Relying on the difference in structure factor between regions with up and down polarization, simulations were carried out in order to test the impact of preferential polarization on the presence of the diffuse satellite peaks. The simulations were based on a periodic domain structure of 5000 domains. The size ratio of domains with up and down polarizations was varied from 90:10 to 10:90. The satellite peak positions and the intensity ratio between the different reflections were determined from the square of the Fourier transform of the spatially varying structure factor for domains of up and down polarizations. All calculated profiles show the diffuse satellite peaks at a fixed ΔQ_x separation from the specular reflection [see Fig. 7(b)]. For a 50:50 size distribution of oppositely polarized domains, corresponding to the perfect stripe state, even order peaks are extinguished. The present simulations indicate that the ΔQ_x position of the

satellite peaks is related to the overall stripe width and not to the widths of the individual up and down domains within one period.

The in-plane symmetry of the satellite peaks was investigated by performing linear Q_x scans for different Φ angles, as illustrated for $\Phi=0-90^\circ$ in Fig. 8 for a 27 unit cell thick sample. The recorded isotropy in ΔQ_x corroborates previous measurements on ultrathin films of $\text{PbTiO}_3/\text{SrTiO}_3$ at temperatures below $\sim 100^\circ\text{C}$, using synchrotron radiation.⁸

Figure 9(a) shows in-plane x-ray scattering profiles of PbTiO_3 on SrTiO_3 for different film thicknesses, i.e., 16, 42, 72, and 94 unit cells, respectively. The satellite peak position is clearly influenced by the film thickness, ΔQ_x increasing with decreasing film thickness, as shown in Fig. 9(a). This trend is observed for samples up to ~ 100 unit cells thick. In Fig. 9(b), the estimated stripe width is plotted as a function of film thickness for samples grown on both SrTiO_3 and Nb:SrTiO_3 . We find that the stripe width is proportional to the film thickness raised to the power of 0.6 ± 0.05 , in approximate agreement with bulk data for KH_2PO_4 (Ref. 5) and BaTiO_3 (Ref. 11), suggesting that the square root dependence of the domain width is valid over six orders of magnitude in crystal thickness, as previously noted by Schilling *et al.*¹¹

Similar thickness dependencies have been previously reported for XRD measurements of PbTiO_3 thin films on SrTiO_3 at higher temperatures.^{7,8} Two phases with characteristically different stripe widths were observed in these ex-

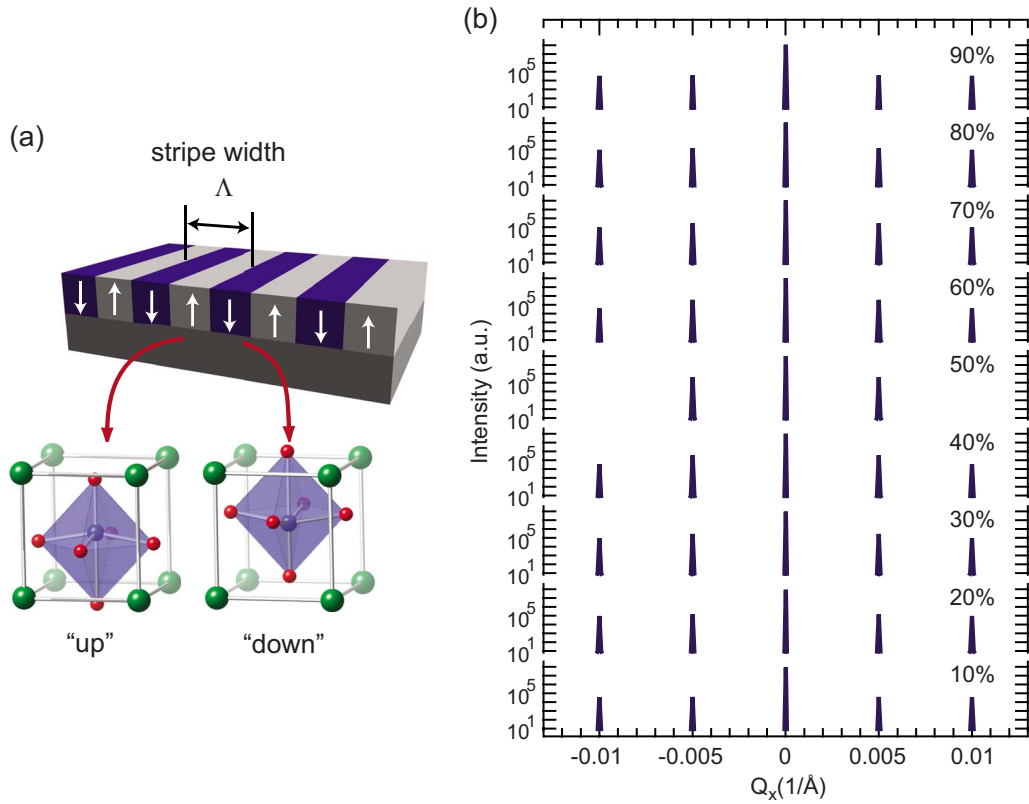


FIG. 7. (Color online) (a) Schematic illustration of the ferroelectric 180° stripe domains. (b) Simulated Q_x profile intensities for $P_{\text{up}}:P_{\text{down}}$ domain size ratios from 10% up to 90% up.

periments: one phase with a small width, dubbed F_α , and one phase with a larger width, dubbed F_β , the domain periodicity being dependent on the film thickness for both phases. For

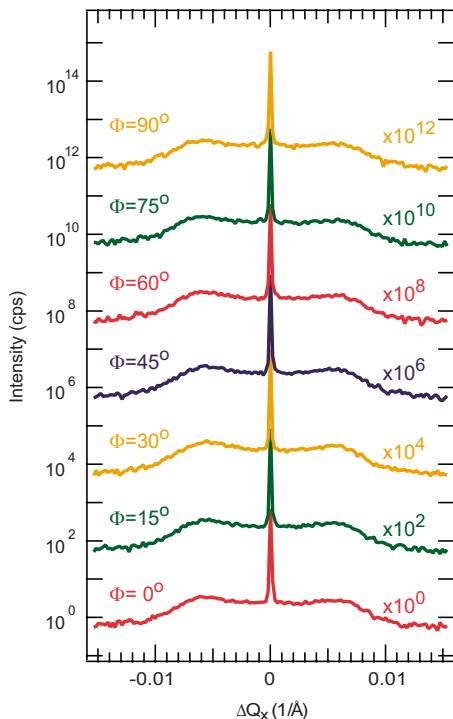


FIG. 8. (Color online) The dependence of the diffuse scattering peaks on Φ for a 27 unit cell thick film of $\text{PbTiO}_3/\text{SrTiO}_3$, recorded around the (001) reflection.

thicker films, the estimated stripe widths in the present experiment exceed those previously reported. For example, the estimated stripe width of a 72 unit cell thick sample at room temperature ($\Lambda=38$ nm) is larger than that reported for both the F_β phase of PbTiO_3 at 600–800 K ($\Lambda=18$ nm) and the F_α phase at 900–950 K ($\Lambda=12$ nm) in Refs. 7 and 8. The published data for the F_β phase of the thinnest samples in Refs. 7,8 was obtained near room temperature, hence the convergence with the present measurements for this phase.

For film thicknesses exceeding approximately 100 unit cells, no clear trends were found. Linear Q_x scans revealed monodomain samples, as judged by the absence of satellite peaks, as well as samples with stripe domains. The stripe domain state is associated with the presence of a nonzero depolarization field. For a thin film with short-circuit boundary conditions the depolarization field is given by^{16,17,32}

$$\varepsilon_d \propto -\frac{P}{d} \propto -\left(\frac{c}{a} - 1\right)^{1/2} \frac{1}{d},$$

where P is the polarization, d is the film thickness, and c/a is the tetragonality of the perovskite unit cell. In Fig. 10, the stripe width is plotted as a function of ε_d , assuming short-circuit conditions across the sample and a similar screening length for the two different substrates. It appears that for depolarization fields larger than a critical value ε_d^* , the measured in-plane stripe width and the depolarization field are correlated. However, for small depolarization fields, there is no clear trend, and monodomain samples are occasionally observed. We note that in this region the characteristic domain size for samples grown on Nb:SrTiO₃ substrate is typi-

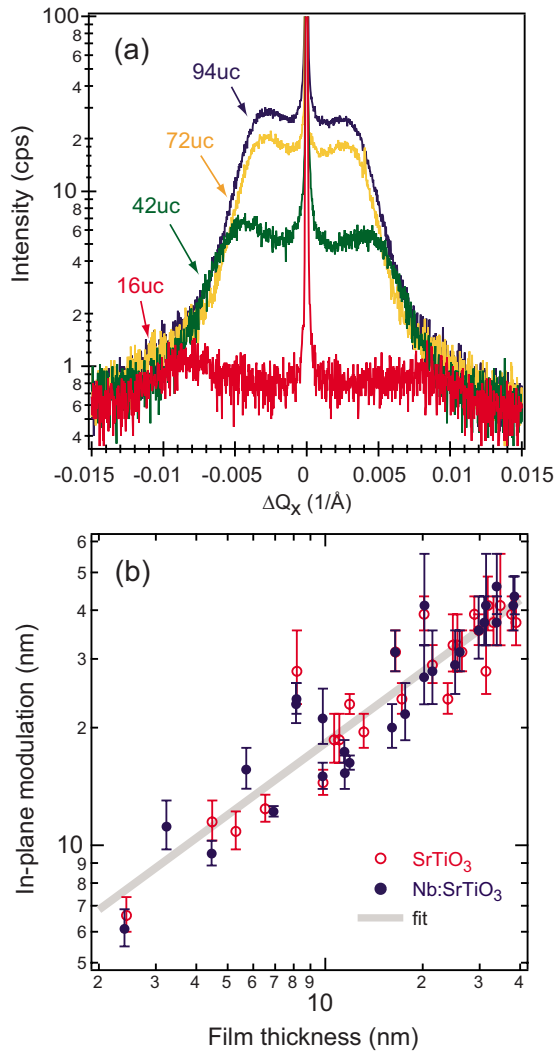


FIG. 9. (Color online) (a) In-plane x-ray scattering profiles for 16, 42, 72, and 94 unit cell thick films of $\text{PbTiO}_3/\text{SrTiO}_3$. (b) Film thickness dependence of the mean stripe width for PbTiO_3 grown on SrTiO_3 and Nb:SrTiO_3 substrates, respectively.

cally larger than for samples grown on SrTiO_3 . It has been reported that monodomain polarization can be obtained by carefully choosing the electrostatic environment,¹⁴ for example, for the $\text{PbTiO}_3/\text{La}_{0.67}\text{Sr}_{0.33}\text{MnO}_3$ system.¹⁵ Hence, it is possible that the conductivity of the substrate influences the domain structure of thick films, although our data suggest that for depolarization fields larger than ε_d^* , possibly dependent on the effective screening length of the substrate, no such difference exists.

Figures 11(a) and 11(b) display linear Q_x -scans recorded with a 1 year interval for PbTiO_3 thin films grown on SrTiO_3 and Nb:SrTiO_3 , respectively. We note that the stripe domain state is retained, and the stripe width unaltered for films grown on Nb:SrTiO_3 . For samples grown on insulating substrate a decrease in ΔQ_x is observed, which indicates that the as grown 21.7 nm domain periodicity was increased (to 26.0 nm) after 1 year of storage in air. In order to assess the impact on the satellite peaks from random variations in domain size and preferential polarization of the stripe domain state, we have run simulations based on a one-dimensional periodic structure of stripe domains (5000 domains) with an

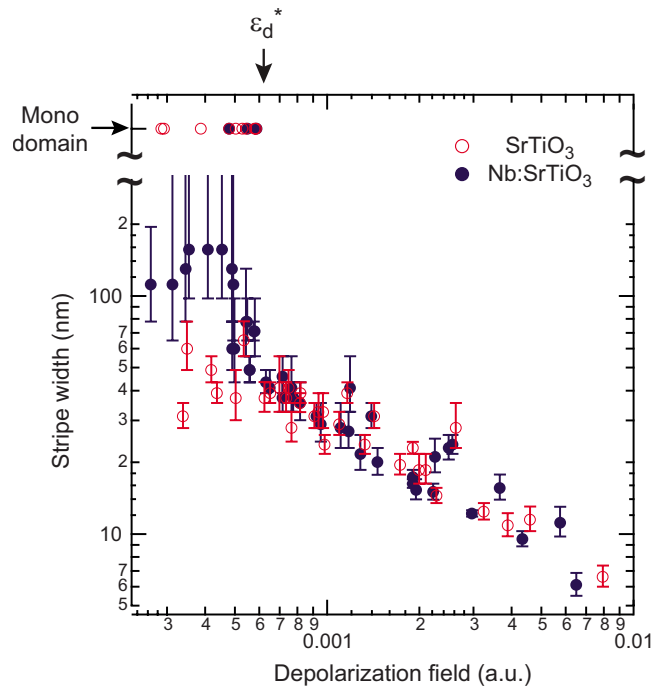


FIG. 10. (Color online) Depolarization field dependence of the stripe width for the ferroelectric stripe domain ground state.

average stripe width of 200 Å. Random variations in the stripe width were introduced by means of an error function, providing an effective stripe width of $200 \text{ \AA} \pm \delta$, where δ was varied from 0 to 200 Å for domain polarization ratios $P_{\text{up}}:P_{\text{down}}$ of 10:90, 20:80, 30:70, 40:60, and 50:50. Figure 12(a) shows the effect of this random variation on the intensity and position of the satellite peak in XRD for a 50:50 size distribution of P_{up} versus P_{down} domains. For a modest random variation in the stripe width, the satellite peak position remains unchanged. However, if the random variations exceed approximately 25% of the in-plane periodicity, ΔQ_x starts decreasing, and the actual stripe width is overestimated. Similar conclusions were reached by Carbone,³³ who found that random variations in domain size may affect the estimate of the periodicity for twin domain structures in manganite films, as obtained from the similar XRD measurements. The satellite-to-specular peak intensity ratio dimin-

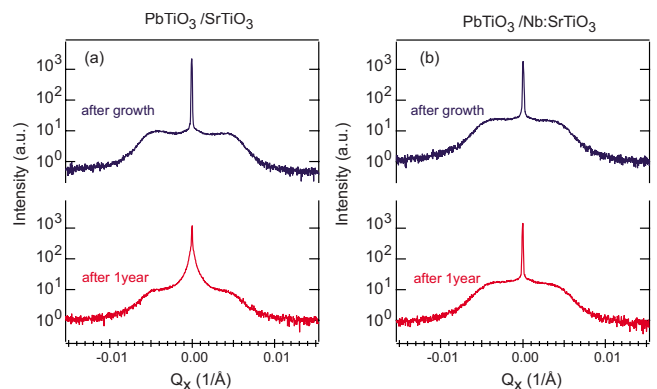


FIG. 11. (Color online) High-resolution linear Q_x profiles of $\text{PbTiO}_3/\text{SrTiO}_3$ (a) and $\text{PbTiO}_3/\text{Nb:SrTiO}_3$ (b), recorded immediately after growth and again after 1 year of storage in air.

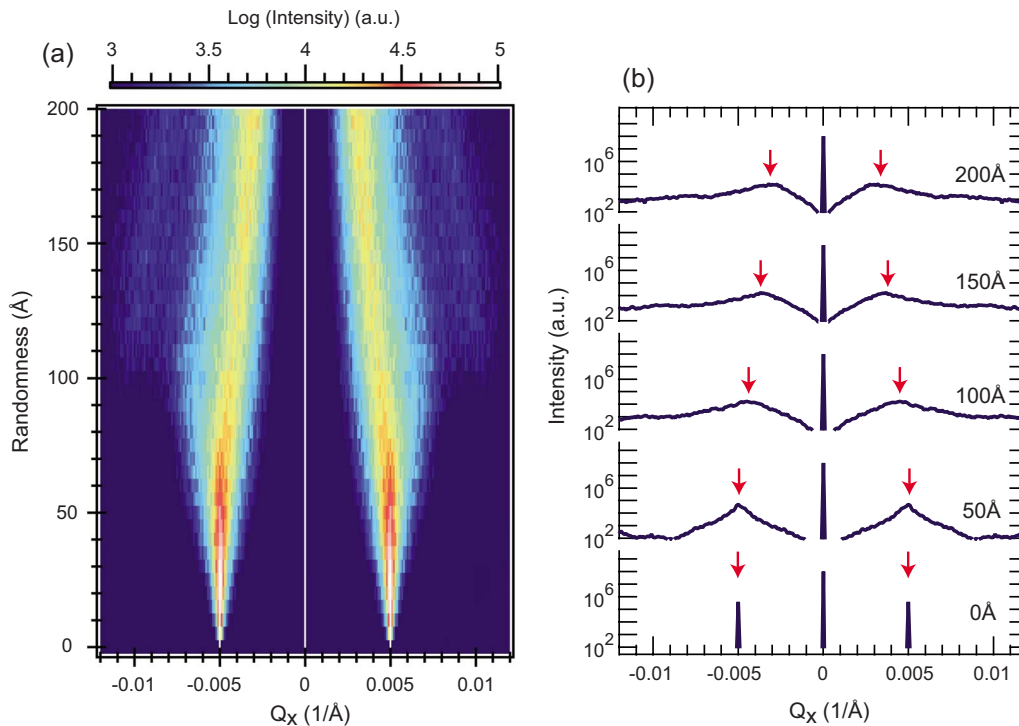


FIG. 12. (Color online) (a) Map of simulated Q_x profiles vs random variations in stripe width for an idéal 50:50 P_{up} vs P_{down} stripe domain state. (b) Corresponding line profiles for 0%, 25%, 50%, 75%, and 100% random variation in stripe width.

ishes. The FWHM of the satellite peak increases upon introduction of statistical variations in the width of the alternate polarization stripe domains, cf. Fig. 12(b) with simulated Q_x linescans for random variations in stripe width up to 0%, 25%, 50%, 75%, and 100% of the statistical mean for an idéal 50:50 (P_{up} versus P_{down}) stripe domain state. The impact on intensity and FWHM of the XRD satellite peak is more pronounced at moderate “domain randomness.” Similar results were obtained for the other P_{up} versus P_{down} domain size distributions. Comparing results from these simulations with the evolution of the satellite peaks for $PbTiO_3/SrTiO_3$, cf. Fig. 11(a), we conclude that the domain randomness of the stripe domain ground state increases with time for $PbTiO_3$ grown on insulating substrate. Furthermore, we note that our stripe width estimates [cf. Fig. 9(b)] increase more sharply with film thickness than reported for the F_α and F_β phases in Refs. 7 and 8. Overestimated stripe widths from a larger domain randomness in our films may contribute to explain this discrepancy.

IV. CONCLUSIONS

We have shown that the satellite peaks associated with the Bragg reflections in XRD measurements on $PbTiO_3$ thin films originate from a bulk effect, and can be attributed to a stripe domain polarization state. Above some threshold depolarization field ϵ_d^* , the average stripe width is controlled by this field. Simulations show that the size ratio of $P_{up}:P_{down}$ domains does not affect the separation ΔQ_x of the satellite peak from the specular Bragg reflection. However, statistical variations in the size of domains bring on a reduction in ΔQ_x for variations exceeding 25% of the average stripe width.

This result implies that the average stripe width is overestimated when the domain size varies across the film surface.

ACKNOWLEDGMENTS

The authors would like to thank the Research Council of Norway for funding via Contract No. 162874/V00. We are indebted to Professors J. Skaar, D. W. Breiby, and Y. Matsumoto for valuable scientific discussions and technical support.

- ¹C. H. Ahn, K. M. Rabe, and J.-M. Triscone, *Science* **303**, 488 (2004).
- ²T. Tybell, C. H. Ahn, and J.-M. Triscone, *Appl. Phys. Lett.* **72**, 1454 (1998).
- ³T. Tybell, C. H. Ahn, and J.-M. Triscone, *Appl. Phys. Lett.* **75**, 856 (1999).
- ⁴T. Tybell, P. Paruch, T. Giamarchi, and J.-M. Triscone, *Phys. Rev. Lett.* **89**, 097601 (2002).
- ⁵T. Mitsui and J. Furuichi, *Phys. Rev.* **90**, 193 (1953).
- ⁶M. E. Lines and A. M. Glass, *Principles and Applications of Ferroelectrics and Related Materials* (Oxford University Press, New York, 1977).
- ⁷S. K. Streiffer, J. A. Eastman, D. D. Fong, C. Thompson, A. Munkholm, M. V. R. Murty, O. Auciello, G. R. Bai, and G. B. Stephenson, *Phys. Rev. Lett.* **89**, 067601 (2002).
- ⁸D. D. Fong, G. B. Stephenson, S. K. Streiffer, J. A. Eastman, O. Auciello, P. H. Fuoss, and C. Thompson, *Science* **304**, 1650 (2004).
- ⁹G. Catalan, A. Janssens, G. Rispens, S. Csiszar, O. Seeck, G. Rijinders, D. H. A. Blank, and B. Noheda, *Phys. Rev. Lett.* **96**, 127602 (2006).
- ¹⁰V. Nagarajan, J. Junquera, J. Q. He, C. L. Jia, R. Waser, K. Lee, Y. K. Kim, S. Baik, T. Zhao, R. Ramesh, Ph. Ghosez, and K. M. Rabe, *J. Appl. Phys.* **100**, 051609 (2006).
- ¹¹A. Schilling, T. B. Adams, R. M. Bowman, J. M. Gregg, G. Catalan, and J. F. Scott, *Phys. Rev. B* **74**, 024115 (2006).
- ¹²R. Takahashi, J. K. Grepstad, T. Tybell, and Y. Matsumoto, *Appl. Phys. Lett.* **92**, 112901 (2008).
- ¹³B.-K. Lai, I. Ponomareva, I. I. Naumov, I. Kornev, H. Fu, L. Bellaiche, and G. J. Salamo, *Phys. Rev. Lett.* **96**, 137602 (2006).
- ¹⁴D. D. Fong, A. M. Kolpak, J. A. Eastman, S. K. Streiffer, P. H. Fuoss, G. B. Stephenson, C. Thompson, D. M. Kim, K. J. Choi, C. B. Eom, I. Grinberg, and A. M. Rappe, *Phys. Rev. Lett.* **96**, 127601 (2006).

- ¹⁵C. Lichtensteiger, M. Dawber, N. Stucki, J.-M. Triscone, J. Hoffman, J.-B. Yau, C. H. Ahn, L. Despont, and P. Aebi, *Appl. Phys. Lett.* **90**, 052907 (2007).
- ¹⁶J. Junquera and P. Ghosez, *Nature (London)* **422**, 506 (2003).
- ¹⁷C. Lichtensteiger, J.-M. Triscone, J. Junquera, and P. Ghosez, *Phys. Rev. Lett.* **94**, 047603 (2005).
- ¹⁸M. Kawasaki, K. Takahashi, T. Maeda, R. Tsuchiya, M. Shinohara, O. Ishiyama, T. Yonezawa, M. Yoshimoto, and H. Koinuma, *Science* **266**, 1540 (1994).
- ¹⁹Ø. Dahl, J. K. Grepstad, and T. Tybell, *J. Appl. Phys.* **103**, 114112 (2008).
- ²⁰J. S. Speck, A. C. Daykin, A. Seifert, A. E. Romanov, and W. Pompe, *J. Appl. Phys.* **78**, 1696 (1995).
- ²¹C. M. Foster, Z. Li, M. Buckett, D. Miller, P. M. Baldo, L. E. Rehn, G. R. Bai, D. Guo, H. You, and K. L. Merkle, *J. Appl. Phys.* **78**, 2607 (1995).
- ²²A. T. J. van Helvoort, Ø. Dahl, B. G. Soleim, R. Holmestad, and T. Tybell, *Appl. Phys. Lett.* **86**, 092907 (2005).
- ²³V. M. Kaganer, R. Köhler, M. Schmidbauer, R. Opitz, and B. Jenichen, *Phys. Rev. B* **55**, 1793 (1997).
- ²⁴JCPDS Card No. 006-0452.
- ²⁵JCPDS Card No. 035-0734.
- ²⁶S. Stemmer, S. K. Streiffer, F. Ernst, and M. Ruhle, *Phys. Status Solidi A* **147**, 135 (1995).
- ²⁷Q. Shen, C. C. Umbach, B. Weselak, and J. M. Blakely, *Phys. Rev. B* **48**, 17967 (1993).
- ²⁸L. Tapfer and P. Grambow, *Appl. Phys. A: Solids Surf.* **A50**, 3 (1990).
- ²⁹C. Thompson, C. M. Foster, J. A. Eastman, and G. B. Stephenson, *Appl. Phys. Lett.* **71**, 3516 (1997).
- ³⁰D.-H. Do, P. G. Evans, E. D. Isaacs, D. M. Kim, C. B. Eom, and E. M. Dufresne, *Nat. Mater.* **3**, 365 (2004).
- ³¹C. A. Wallace, *J. Appl. Crystallogr.* **3**, 546 (1970).
- ³²H. Morioka, S. Yokoyama, T. Oikawa, H. Funakubo, and K. Saito, *Appl. Phys. Lett.* **85**, 3516 (2004).
- ³³G. Carbone, Ph.D. thesis, Institut für Theoretische und Angewandte Physik der Universität Stuttgart, 2004.